Vol. 22, n.° 1, enero-junio de 2024
ISSN impreso: 1657-6527 • ISSN en línea: 2145-8502

FUENTES
EL REVENTÓN ENERGÉTICO

A NEW APPROACH TO PREDICT THE CASCADE EFFECT IN TURBINE FLOWMETERS APPLIED TO LIQUEFIED PETROLEUM GAS

UN NUEVO ENFOQUE PARA PREDECIR EL EFECTO CASCADA EN CAUDALÍMETROS DE TURBINA APLICADOS A GAS LICUADO DE PETRÓLEO

Tiago Miranda Pereira; Jerson Rogério Pinheiro Vaz

Federal University of Pará, Graduate Program in Natural Resources Engineering, Av. Augusto Correa, N 1, Belém, PA 66075-900, Brazil.

tiagopereira@ufpa.br

Recibido: 15 de marzo de 2024. Aprobado: 19 de agosto de 2024. Versión final: 17 de septiembre de 2024.

Abstract

The measurement of transferred quantities of liquid products is essential in multiple industrial activities. Turbine flowmeters are largely employed, especially in custody transferring applications, due to their high accuracy and wide operational range. Analysis and improvement of turbine meters behaviors require specialized mathematical tools, once the constructive characteristics of multiple blades impose challenges to the determination of lift and drag coefficients. The appliance of the integral method Blade Element Theory (BET) without the evaluation of the cascade effect can lead to overestimation of turbine performance. The present work proposes an innovative and semi empirical cascade effect correction within the BET model to estimate the hydrodynamic behavior of turbine flowmeters in a Liquefied Petroleum Gas (LPG) plant. The model provides a strategy to correct the cascade effect on the rotor annular section, accurately predicting lift and drag coefficients at various blade sections. Operational parameters of the studied turbines, obtained from computer modeling, are compared to field data of an existent plant, in several conditions. Computational fluid dynamics (CFD) techniques are employed for the analysis. The validation of CFD model comprises the comparative analysis between numerical results and in-situ data acquired in the regular operation of the measurement system. The results indicate that the proposed model based on BET is able to predict the turbine flowmeter performance and provides precise estimative for field results of angular velocity and linearity.

Keywords: Turbine flowmeter; Computational Fluid Dynamics; Blade Element Theory; Cascade effect; Liquefied Petroleum Gas

Como citar: Pereira, T. M, & Vaz, J. R. P. A new approach to predict the cascade effect in turbine flowmeters applied to liquefied petroleum gas. *Fuentes, El Reventón Energético*, *22*(1), 79-97. https://doi.org/10.18273/revfue.v22n1-2024006

Resumen

La medición de cantidades transferidas de productos líquidos es fundamental en múltiples actividades industriales. Los caudalímetros de turbina se emplean ampliamente, especialmente en aplicaciones de transferencia de custodia, debido a su alta precisión y amplio rango operativo. El análisis y la mejora del comportamiento de los medidores de turbinas requieren herramientas matemáticas especializadas, una vez que las características constructivas de múltiples palas imponen desafíos para la determinación de los coeficientes de sustentación y resistencia. La aplicación del método integral Blade Element Theory (BET) sin la evaluación del efecto cascada puede conducir a una sobreestimación del rendimiento de la turbina. El presente trabajo propone una innovadora corrección del efecto cascada dentro del modelo BET para estimar el comportamiento hidrodinámico de caudalímetros de turbina en una planta de Gas Licuado de Petróleo (GLP). El modelo proporciona una estrategia para corregir el efecto de cascada en la sección anular del rotor, prediciendo con precisión los coeficientes de sustentación y resistencia en varias secciones de la pala. Los parámetros operativos de las turbinas estudiadas, obtenidos a partir de modelos informáticos, se comparan con datos de campo de una planta existente, en varias condiciones. Para el análisis se emplean técnicas de dinámica de fluidos computacional (CFD). La validación del modelo CFD comprende el análisis comparativo entre los resultados numéricos y los datos in situ adquiridos durante el funcionamiento normal del sistema de medición. Los resultados indican que el modelo propuesto basado en BET es capaz de predecir el rendimiento del caudalímetro de la turbina y proporciona una estimación precisa de los resultados de campo de velocidad angular y linealidad.

Palabras clave: Caudalímetro de Turbina; Dinámica de Fluidos Computacional; Teoría del Elemento de Pala; Efecto Cascada; Gas Licuado de Petróleo.

1. Introduction

Turbine flowmeters are very important measurement devices. They are widely employed in industrial process control, oil and gas custody transferring and other fields. These types of meters usually have high accuracy, good repeatability, wide rangeability and other advantages (Guo et al., 2013). Turbine meters work based on the flow kinetic energy, which promotes spinning of the turbine while the flow rate can be measured according to the angular velocity of the rotor (Control INC, 2005). The flow rate is calibrated with the angular velocity of the turbine flowmeter, in order to give an accurate measurement. Considering the turbine meter rotational principle of working and its constructive characteristics, it is identified the possibility of implementing modeling techniques classically developed to the study of wind and hydraulic turbines. Generally, wind and hydraulic turbines are applied to energy generation purposes, in the study of measurement turbine behavior, aiming to amplify the comprehension about the factors that can interfere in their performance.

Due to turbine flowmeter large acceptance in industry, the study of such devices gained space in scientific publications. For example, Salami (1984) developed a model to predict the effect of velocity profile and swirl on the flowmeter calibration curve. Baker (1991) organized and published a wide revision about available information related to turbine flowmeters, initially based on technical data from manufacturers, including constructive aspects, operational characteristics, influence of variations of fluid and flow properties on the meter performance and maintenance recommendations to promote good durability. Xu (1992a) proposed a model to calculate the aerodynamic characteristics of turbine flowmeter blades. His model is developed from the simulation of dimensions of separated flow regions in leading edge for different angles of incidence, using transient method to predict vortex distribution. Xu (1992a) used the same method to simulate the behavior of the wake formed in trailing edge, through which he calculated the lift and drag coefficients. Also, Xu (1992b) published a model to predict turbine flowmeter performance using the results from the previously cited paper. His new model is an iterative calculation of the angular velocity that promotes balance between propulsive and dissipative torques. His results revealed good agreement with experimental data, especially in the absence of upstream swirl. In another work, Baker (1993) contributed to the state of the art with the organized collection of theoretical and experimental works related to this type of meter.

A method to evaluate turbine flowmeter performance with computational fluid dynamics (CFD) techniques is proposed by Saboohi et al. (2015). In their model, a CFD simulation to predict the calibration curve of the meter is carried out, where resistive torque due to the sliding bearing is modeled with an algorithm based on the finite difference method. The comparative analysis between their results and experimental data revealed maximum error of 2.95 % for oil flow simulation and 4.58 % for water flow. Hariri et al. (2015) also applied CFD to analyze the effect of operational parameters and flow perturbations in the accuracy of

an industrial turbine flowmeter employed in crude oil transferring. The model is able to predict the behavior of the angular velocity with the increase of density and viscosity. In addition, it is detected great sensibility to deformations on upstream velocity profiles. Dzemic et al. (2018) investigated the dynamic response of turbine flowmeters to abrupt transitions on gas flow regime induced by rapid closing and reopening of valves. Their experimental results confirmed that turbine flowmeter is able to rapidly respond to acceleration, but during deceleration regime the response is much slower and that causes over-registration of gas volume. Most recent publications confirm versatility and accessibility of turbine flowmeters. Wang et al. (2020) applied a turbine flowmeter to the development of a method to interpret water flow rate in a complex three-phase flow oil-airwater typically found in oil production fields. Their method presents good behavior valid for laboratory use under ideal conditions. Caldas et al. (2020) developed and manufactured a meter capable to operate in measurement of lithium bromide salt solution. The meter is very effective since the results are very close to the measurements with errors less than 4 %. Although there are several works available in the current literature on turbine flowmeters, the authors are unaware of any study on the consideration of the cascade effect in rotors with multiple blades.

Typically, hydraulic blades are subjected to boundary layer separation, which can impact the flow around turbine rotor and, consequently, the hydrodynamic performance of the blade (Limacher et al., 2016; Limacher & Rival, 2015). Such boundary layer separation is associated to a vortex formation (Andriotis et al., 2008) along of the shape of a hydrofoil (Ji et al., 2014). Turbine flowmeters employed in industrial process control usually present multiple blades, and they are lift-based axial-flow turbines, having the same physical principles similarly to hydrokinetic rotors (Laws & Epps, 2016). Axial turbines can be modeled through the well-known Blade Element Theory (BET) (Silva et al., 2018), which generally agrees well with experimental data (Moreira et al., 2020). Furthermore, BET has low computational cost and easy numerical implementation when compared to CFD techniques, as further explained in Vaz & Wood (2016).

In the present work, BET is applied to the study of hydrodynamic behavior of a turbine flowmeter, including the calculation of cascade effect correction, in order to accurately predict lift and drag coefficients at each blade section. Such application, along with dynamic equation of meter movement and CFD modeling leads to the development of a technique for the analysis of turbine operational performance. The calculation of the expected angular velocity corresponds to each flow rate of the transferring fluid, within the operational range. The technique reveals an innovative approach regarding the methodologies of analysis available on technical and scientific literature related to turbine flowmeters. In addition, it is noteworthy that the study is applied to the measurement of Liquefied Petroleum Gas (LPG), which is a fluid not much considered in the available studies about operational behavior of turbines.

2. Numerical methodology

2.1. Dynamic model of turbine flowmeter

The dynamic system of the studied turbine flowmeter consists of a hydrodynamic rotor with 12 blades and mass momentum of inertia J_T assembled on a stator shaft. Between the rotor and the shaft there is a sliding bearing.

The dynamic equation for the meter is (Vaz et al., 2018)

$$T_T - T_D = J_T \frac{d\omega_T}{dt}, \tag{1}$$

where T_T is the hydrodynamic torque resulted from the combination of lift and drag forces throughout the turbine blade, T_D is the dissipative torque, ω_T is the turbine angular velocity and t is time. In the present work, T_T is calculated using the BET, which is detailed in subsection 2.2. The dissipative torque, T_D , is determined by the classic Petroff's (1883) equation, as given by Shigley (1963),

$$T_D = \frac{2\pi {r_b}^3 l \mu \omega_T}{e}, \tag{2}$$

where r_b is the rotor inner radius, l is the rotor width, μ is the dynamic viscosity of the lubricant, in this case LPG, and e is the clearance between the rotor inner wall and the sleeve outer face.

2.2. Blade element theory

BET is widely used in horizontal axis turbine design considering uniform free flow. It is essentially an integral method, with semi-empirical information of hydrodynamic forces in blade sections obtained from a two-dimensional model of airfoil flow combined with experimental data for section lift and drag (Silva et al., 2017). However, once the turbine flowmeter, described in the present work, operates confined in a duct, the velocity profile approaching the turbine rotor is deformed and, consequently, there is the necessity to consider such deformation in BET. This deformation is further detailed in Rio Vaz et al. (2018), as for a ducted hydrokinetic turbine the flow changes the turbine behavior. In this way, it is proposed an extension to BET method to the case of confined turbines without hydrodynamic loading, in which a correction for the cascade effect is proposed. This model consists in a quasi-steady approach, as it couples the BET to the dynamic equation through Eq. 1, which calculates the hydrodynamic torque along the rotor blade. Figure 1 illustrates the velocity profile deformation while approaching the turbine blades.

The turbines employed in energy generation applications promote interference on the fluid flow passing through the rotor by means of the loading imposed by the system, as for example an electric generator. As a consequence, axial and tangential induction factors, a and a', are different from zero. However, in the case of a turbine flowmeter, the aim is not energy generation, but the rotation, from which the flow rate can be determined. In this way, a turbine flowmeter has null loading over the axis, making the blades to be stationary, as further described by Wood (2011). This leads to the condition $a \sim a' \sim 0$. With this condition, the BET method adapted to the case of turbine flowmeters can be described. Thus, considering the velocities triangle and the hydrodynamic loads of lift and drag in each turbine blade section shown in Figure 2, normal and tangential forces over the rotor are determined, as

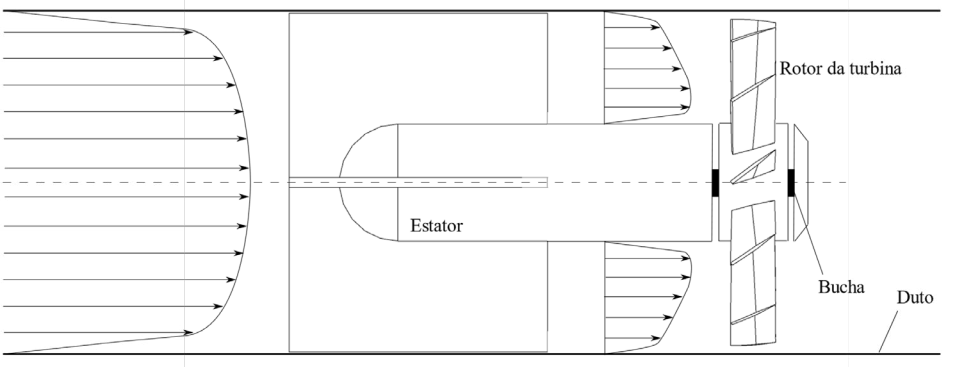

Figure 1. Radial variation of the velocity profile close to the turbine blades.

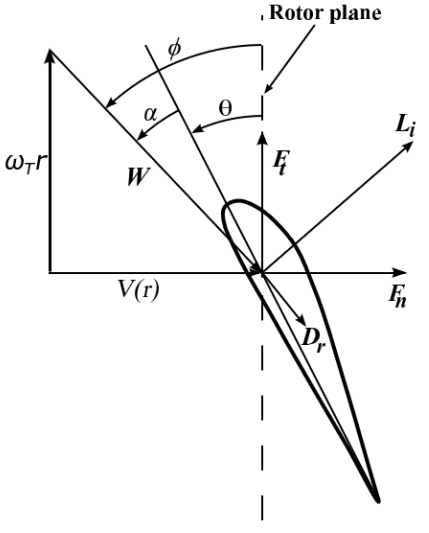

Figure 2. Velocities diagram and hydrodynamic loading in each blade section.

$$F_n = L_i \cos\phi + D_r \sin\phi \quad (3)$$ and

and

$$F_t = L_i \sin\phi + D_r \cos\phi, \quad (4)$$

where F_n is the normal force, F_t is the tangential force, and L_i and D_r are lift and drag forces, respectively, while ϕ is the flow angle. Also, in Figure 2, α is the angle of attack, θ is the twist angle, $V(r)$ is the axial velocity, W is the relative velocity, and r the radial position.

Normalizing Eqs. 3 and 4 by the term $\frac{1}{2}\rho W^2 c$, C_n and C_t are

$$C_n = C_l \cos\phi + C_d \sin\phi \quad (5)$$

$$C_t = C_l \sin\phi - C_d \cos\phi\,, \quad (6)$$

where

$$C_n = \frac{F_n}{\frac{1}{2}\rho W^2 c} \quad (7)$$

and

$$C_t = \frac{F_t}{\frac{1}{2}\rho W^2 c} \quad (8)$$

W, the relative velocity at each section of the turbine blade, is given by

$$W = \sqrt{V^2(1-a)^2 + \omega_T^2 r^2 (1+a')^2}\,, \quad (9)$$

where V is the upstream velocity, ω is the angular velocity, a and a' are the axial and tangential induction factors, respectively. As previously mentioned, the turbine blades are stationary, leading a and a' to be very small (Vaz et al., 2018; Wood, 2014). So, Eq. 9 becomes

$$W = \sqrt{V^2 + \omega_T^2 r^2}. \quad (10)$$

From the forces per unit of length F_n and F_t, the thrust and torque on the control volume with width dr, shown in Figure 3, are:

$$dE_T = BF_n dr \quad (11)$$

and

$$dT_T = BrF_t dr, \quad (12)$$

where B is the number of blades. Substituting Eqs. 7 and 8 in Eqs. 11 and 12, respectively, the equations for the hydrodynamic thrust and torque of the turbine are obtained,

$$E_T = \frac{1}{2}\rho B \int_{r_h}^{R} W^2 c C_n dr \quad (13)$$

and

$$T_T = \frac{1}{2}\rho B \int_{r_h}^{R} W^2 c C_t r dr\,, \quad (14)$$

where r_h is the radius of the hub, and R is the radius of the rotor.

Substituting Eq. 14 in the dynamic equation of the turbine meter, Eq. 1, it gives

$$J_T \frac{d\omega_T}{dt} - \frac{1}{2}\rho B \int_{r_h}^{R} W^2 c C_t r dr + T_D = 0. \quad (15)$$

The operational conditions simulated in the present work occur in steady state regime. Consequently, the angular velocity does not vary with time and the first term of Eq. 15 is zero. So, the equation is rewritten as

$$\frac{1}{2}\rho B \int_{r_h}^{R} W^2 c C_t r dr + T_D = 0. \quad (16)$$

As the parameters W, C_t and T_D are functions of the turbine angular velocity ω_T, Eq. 16 can be easily solved through interactive numerical methods. For each iteration, the hydrodynamic torque is calculated by the BET method and the dissipative torque from Eq. 2.

The methodology adopted in the present work is illustrated in Figure 4.

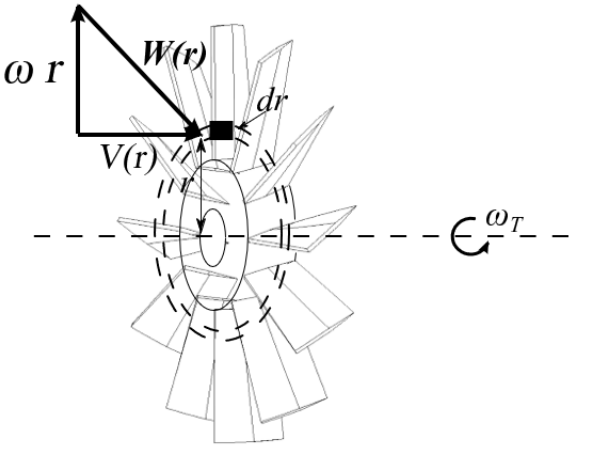

Figure 3. Infinitesimal control volume with width *dr.*

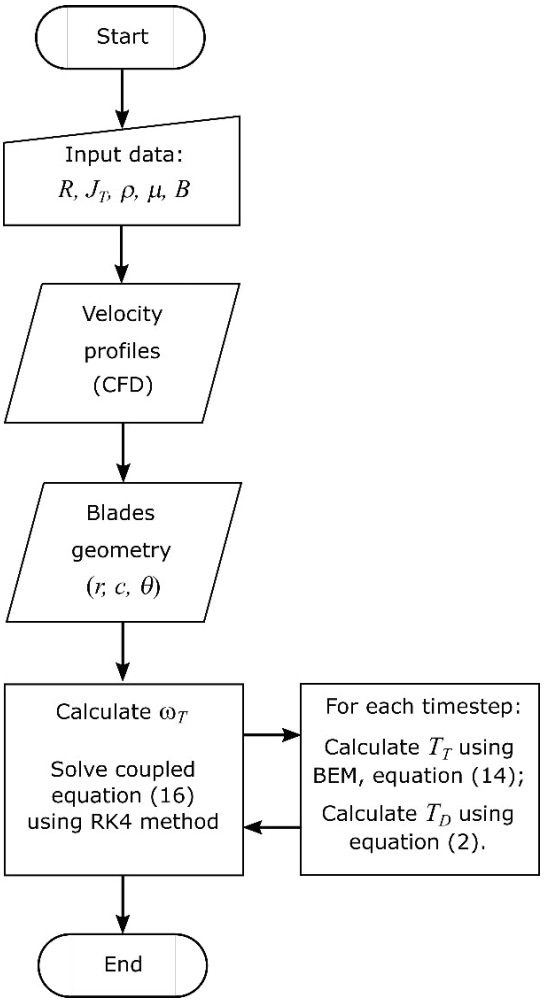

Figure 4. Numerical methodology flowchart.

2.3. Cascade effect correction

The studied turbine flowmeter consists of a multiple blade rotor. The hydrofoil shape of the blades is represented in Figure 5. For this kind of rotor, it is necessary to consider the cascade effect resultant of the proximity between the 12 blades. This effect has been a challenge for turbine theories due to the scarceness of reliable models in the literature, aiming the adequate corrections to the lift and drag parameters in turbines with multiple blades. The complexity of flow fields around cascades is important, making the development of mathematical tools to accurately predict lift and drag coefficients a major concern.

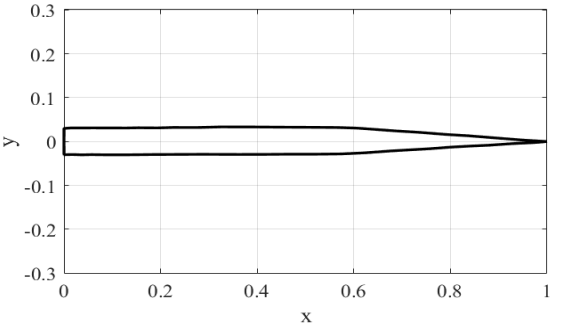

Figure 5. Foil profile coordinates.

Fagbenro (2013) developed a study, using CFD, on the effect of the increase in number of blades in rotors over the lift and drag coefficients of a multiple blades turbine employed in water supply. In the turbine, the foils where constructed with curved plates. Figure 6 shows the main result obtained by Fagbenro (2013). It is observed that the lift coefficient considering the solidity σ = 1.5 can be up to 57 % smaller for a 10° angle of attack. This result shows how much the cascade effect impacts lift and drag forces in turbines with high number of blades. The local solidity, σ, is defined as

$$\sigma = \frac{Bc}{2\pi r} \ , \qquad (17)$$

The increase in solidity leads to lift and drag reductions, becoming the behavior prediction of turbine flowmeter through BET a big challenge. Considering the constructive characteristics of the blade foil studied, the blade profile is modelled as a flat plate, and the formulations described by Wood (2011) for a flat plate are adopted:

$$C_l = 2\,sin\,\alpha\,cos\,\alpha = \ sin(2\alpha); \qquad (18)$$

$$C_d = 2\,sin^2\,\alpha = 1 - cos(2\alpha). \qquad (19)$$

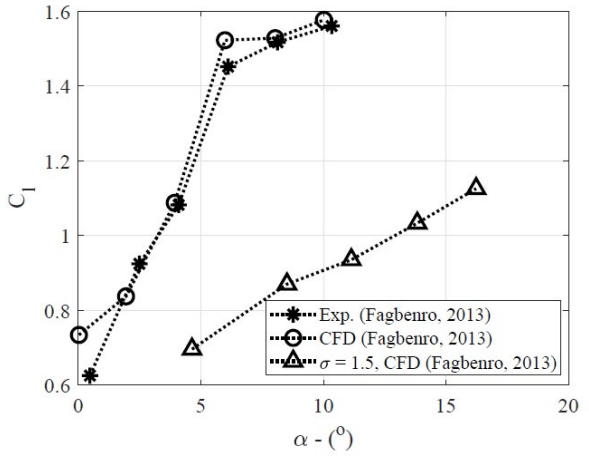

Figure 6. Lift coefficient for curved plates airfoil (Fagbenro, 2020).

Now, a correction for the cascade effect to the values of lift and drag coefficients given by Eqs. 18 and 19 needs to be done. In this case, the corrections are based on formulations to the effect of boundaries in wind tunnels. These formulations, as described in Selig et al. (1995), are applied as a consequence of flow confinement in reduced sections, which promote alterations of lift and drag coefficients on a given airfoil due to the proximity from inner walls in tunnels. The corrections for lift and angle of attack are:

$$\Delta C_{lc} = \sigma_c C_l. \tag{20}$$

$$\Delta\alpha_c = \frac{57{,}3\sigma_c}{2\pi}\left(C_l + 4C_{m,c/4}\right), \tag{21}$$

where

$$\sigma_c = \frac{\pi^2}{48}\left(\frac{c}{h_{ts}}\right)^2, \tag{22}$$

being h_{ts} the test section height, which here is assumed to be equal to the distance between two adjacent blades, i.e.

$$h_{ts} \approx \frac{2\pi r}{B} = \frac{c}{\sigma}. \tag{23}$$

The corrected angle of attack, α_c , is assumed to be

$$\alpha_c = \alpha_u - \Delta\alpha_c, \tag{24}$$

where α_u is the uncorrected angle for an isolated hydrofoil. Proper rearrangement of Eqs. 17 and 21 to 24, for $C_{m,c/4} = 0$, leads to

$$\alpha_c = \alpha_u - k_c(\sigma)^2 C_l, \tag{25}$$

where k_c is a dimensionless constant related to the geometric shape of the hydrofoil, which modifies the curvature of the streamlines passing between blades. Then, the lift and drag coefficients for a flat plate corrected due to the cascade effect are given by:

$$C_{lc} = sin(2\alpha_c); \tag{26}$$

$$C_{dc} = 1 - cos(2\alpha_c). \tag{27}$$

2.4. CFD simulation

In order to obtain the velocity profiles of the flow in the region of approximation to the contact with the turbine blades, a numerical modeling is used, applying the commercial software ANSYS CFX. The geometry of the model is constructed based on the dimensional characteristics of the studied turbine meter, which consists in a 4 inch diameter industrial flow meter with 12 blades (Daniel Measurement and Control, Inc., 2005). The blade shapes have specific twist that provide a particular angle of attack for each radial section of the rotor. Overall geometry aspects are illustrated in Figure 7. The radial distributions of chord and twist angle of the blades are presented in Table 1.

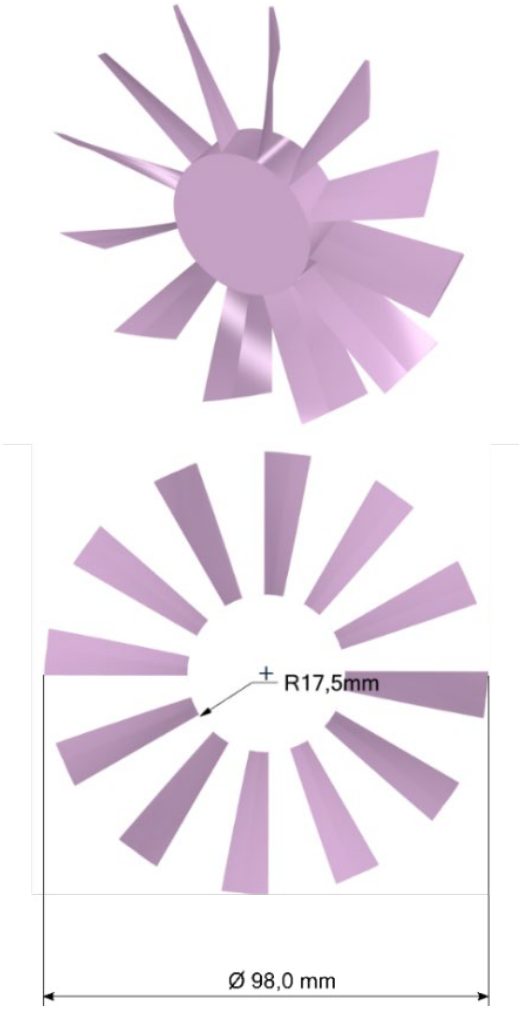

Figure 7. Turbine meter model geometry.

Table 1. Radial distributions of chord and twist angle

r (mm)	*c* (mm)	θ (°)
17.7	13.29	16.98
21.0	13.68	19.22
24.3	13.87	22.34
27.6	14.20	24.74
30.9	14.51	26.85
34.3	14.94	29.34
37.6	15.30	31.30
40.9	15.70	33.13
44.2	16.11	34.84
47.5	16.46	36.55

Aiming the reduction of computational time consuming, and assuming that axisymmetric modeling is reasonably applicable, in view of ducted construction of the turbine meter assembly, it is adopted the periodic concept of modeling, in which only 1/12 of the domain is drawn, and the appropriate interfaces are configured.

With the objective of reproducing the flow conditions provided in the industrial facility, the inlet stator, that delimits an annular region for the flow in the immediate proximities of the turbine, is considered in the geometry construction. Also, straight pipe segments before and after the meter are modelled, having 3D length for the upstream and 4D length for the downstream segment, being D the diameter of the flowmeter. Figure 8 illustrates the total fluid domain, where the 12 instances of the computational model are visualized to enhance comprehension.

In the CFD modeling developed in this work, the computational domain is divided into three sub-domains, consisting of upstream, rotational and downstream zones. The intermediate zone is considered as moving while the others are stationary zones. Frozen Rotor approach is used to simulate the rotary zone and its interaction with upstream and downstream segments. This approach is proven to be more accurate to study turbine meter performance as described in Hariri et al. (2015).

Pressure is imposed at the outlet, once this operational parameter can be measured by field instrumentation. At the inlet, fully developed velocity flow is considered, and the turbulent velocity profile is defined. The mean velocity is obtained from continuity equation, considering that inner diameter and average volumetric

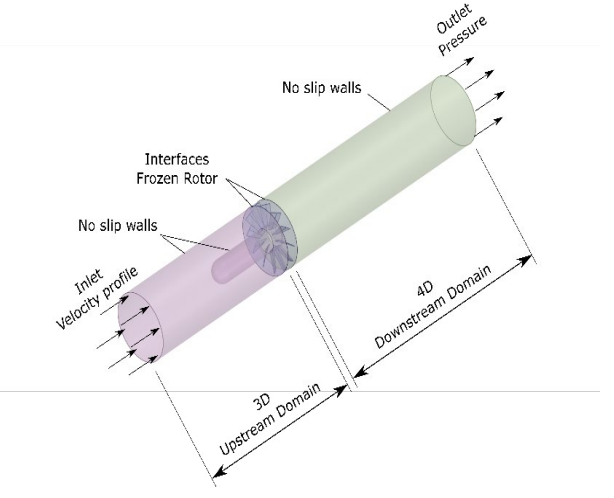

Figure 8. Fluid domain and boundary conditions.

flow rate for a given steady state operational condition are known. The turbulent velocity profile is set up using the power law, as presented in Brennen (2016),

$$u = U\left(1 - \frac{r}{R}\right)^{\frac{1}{n}}. \qquad (28)$$

where u is the axial component of the velocity vector, U is the centerline velocity, r is the radial position, R is the internal pipe radius and n is a parameter dependent of the Reynolds number. The Reynolds number for the operational conditions simulated in the present work varies from 1.2×10^5 to 4.2×10^5, so $n = 7$ is considered.

No-slip boundary condition is set up for all walls. In addition, walls are considered smooth, especially because in the region of interest, there are blade surfaces and flowmeter body inner wall, that in fact, give smooth aspects to the surfaces in contact with the fluid.

Unstructured tetrahedral mesh is adopted to build the fluid domain, except the blades immediate vicinities, where prismatic layers are positioned by means of inflation algorithms available in the CFD pre-processing interface, with the purpose of better represent the boundary layer region. The meshing interface of software ANSYS CFX is used to generate the mesh grid. The number of elements adopted, after mesh convergence study, is 343,935, distributed as follows: 80,008 elements for upstream domain, 139,673 elements for rotational domain and 124,254 elements for downstream domain. Figure 9 exhibits the mesh grid of the whole fluid domain, pointing out the mesh refinement through the cross section visualization at the region of interest. It is worth noting that the mesh is especially refined around the blades proximities. Figure 10 shows the structured prismatic layers arranged around the blades.

The flow is considered incompressible and entirely turbulent. The turbulence is modeled through the so-called $k - \omega$ SST model. Automatic wall function of $k - \omega$ SST in ANSYS CFX is used to predict near-wall fluid behavior. The High Resolution Scheme is selected to the advection term, which is a nonlinear method of correction applied to the UPWIND scheme. For turbulence equations, High Resolution advection scheme is also used. The convergence criteria is set for all variables and the residuals are less than 10^{-4}. Considering that, in the studied industrial facility, the flowmeter works practically with stabilized operational variables during all the transferring operations, and the analysis is carried out for steady state conditions.

The LPG properties are shown in Table 2.

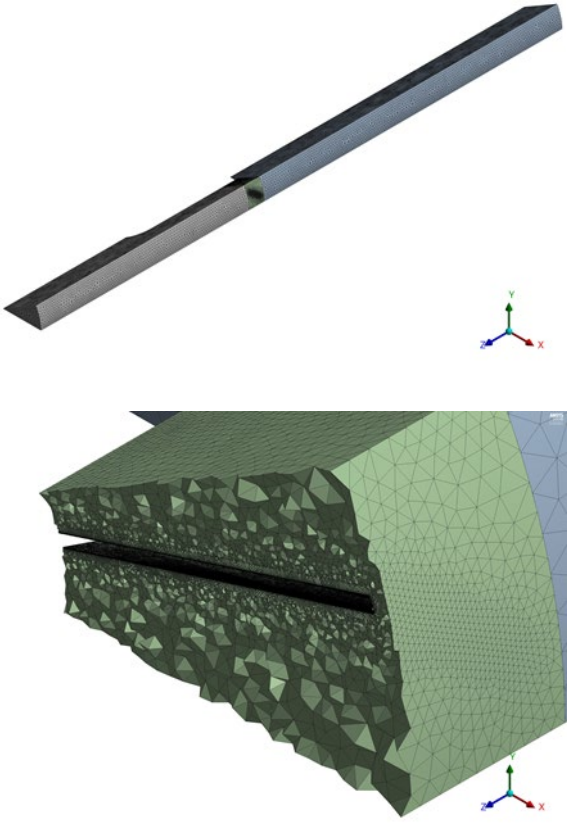

Figure 9. Mesh grid visualization with refinement of flowmeter region.

Table 2. Physical properties of LPG considered in the CFD simulations.

Fluid	Density (kg/m^3)	Molar mass (kg/kmol)	Viscosity (Pa.s)
LPG (liquid phase)	581.22	---	0.0001978

All the numerical solutions described in this paper are performed with Intel R Core™ i7-10510U computer, with 2.3 GHz processor and 16 GB RAM. Furthermore, serial CPU processing is used in all simulations.

3. Results and discussion

3.1. Operational conditions

The physical setup of the simulations is defined based on the operational parameters measured by calibrated field instrumentation during industrial usage. These parameters are listed in Table 3. Details of the turbine flow meter setup can be visualized in Figure 11.

From the basic theory of turbine flowmeters, the angular velocity of the rotor is directly proportional to the fluid velocity through the turbine. This proportionality is expressed by a factor, called k-factor, in pulses/m^3, obtained from Eq. 29, where Q is the flow rate.

$$\text{k-factor} = \frac{B\omega_T}{2\pi Q} \tag{29}$$

Turbine meters have a nominal k-factor, which is, in theory, constant to a given geometry. In practice, k-factor changes at different operational conditions. As a consequence, turbine flowmeters are subjected to performance tests in a specific range of flow rates in which the operational range of the meter is defined. Chapter 5 of the API Manual of Petroleum Measurement Standards (API MPMS) [29], a publication from the American Petroleum Institute (API) dedicated to design criteria, based on the best industrial practice for the custody transfer metering of liquid hydrocarbons, establishes recommended practice to this test. According to API MPMS Chapter 5.3 [29], turbine measurement results are compared in real time to the volume flow rate attained by a prover, in-situ, connected in series with the meter, and the corresponding k-factor is calculated by a flow computer. The k-factors in Table 3 are obtained in real proving test of the studied turbine meter. The six values of flow rate are adjusted, and after stabilized operational parameters are reached, proving runs are performed and the k-factor is registered.

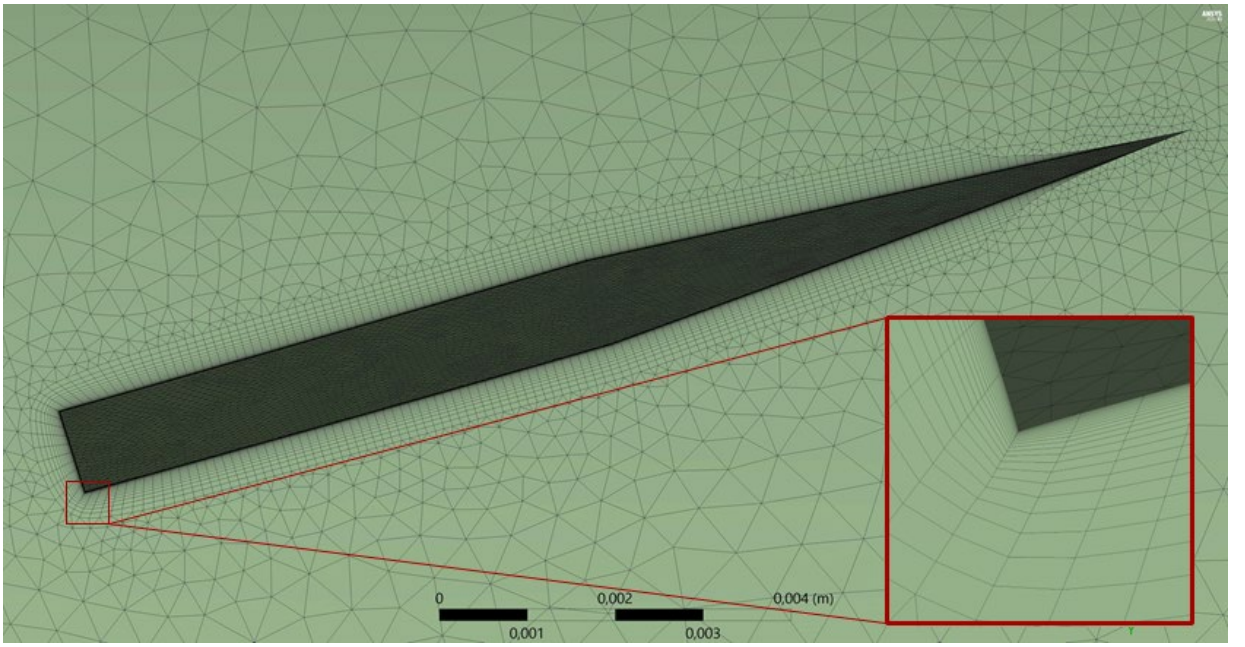

Figure 10. Structured prismatic mesh in blades surrounding.

Table 3. Operational parameters setup.

Set	Flow rate (m^3/h)	k-factor ($pulses/m^3$)	Inlet mean velocity (m/s)	Angular velocity (rad/s)	Outlet pressure **(kPa)**
1	80	3193.119	2.7	37.15	1490.61
2	120	3195.473	4.1	55.77	1529.84
3	160	3196.339	5.5	74.38	1490.61
4	200	3196.479	6.9	92.98	1549.45
5	240	3195.642	8.2	111.55	1490.61
6	280	3195.857	9.6	130.15	1392.54

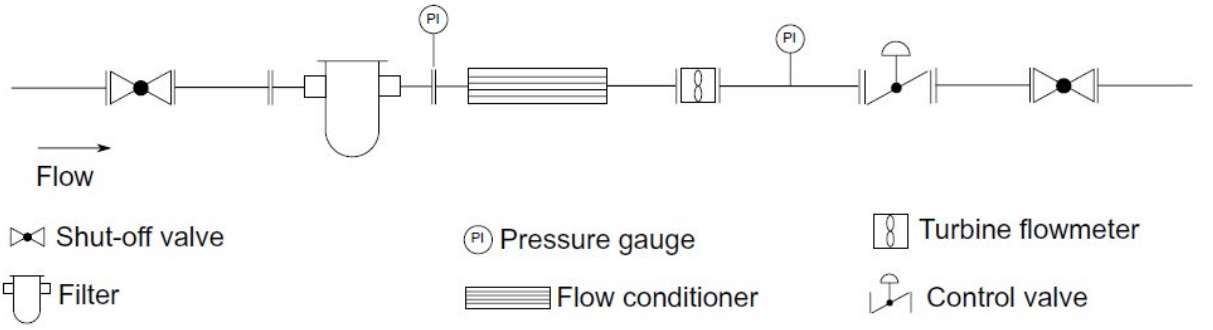

Figure 11. Turbine flowmeter installation.

Knowing the k-factor, the flow rate and the geometrical characteristics of the measurement system, the parameters inlet mean velocity and angular velocity in Table 3 are related to each other through the appropriate use of Eq. 29 and the applicable consistence of units. The outlet pressure is attained by the field measurement and it is used as input data in the simulation.

3.2. Mesh convergence study and model validation

Considering the influence of mesh size in the numerical results of the CFD simulation, a mesh refinement study is conducted to evaluate the most appropriate mesh size distribution to the present analysis. Initially, overall cell size is analyzed based on the model capability to provide the velocity profile inside the pipe with acceptable independence from the mesh refinement.

The operational condition chosen to perform the mesh convergence study is the case 1 in Table 3, i.e., flow rate of 80 m^3/h. Four different element sizes are simulated and the velocity profile in a pipe section located 200 mm downstream the turbine blades trailing edge is obtained from CFD results, as shown in Figure 12(a). The comparative results, in Figure 12(b), presents the velocity distribution in a longitudinal plane that intersects the turbine blade. The vertical red line indicates the position where the velocity profiles are collected. Figure 12(a) also illustrates the vortex region downstream the turbine stator that explains the distortion in the velocity profiles for r < 25 mm. In Figure 12(b), it is possible to observe that only a small variation in velocity profile is perceived from Mesh C to Mesh D. To demonstrate the mesh refinement employed, the velocity profiles $u(r)$ are quantitatively compared using the infinity norm $\|u(r)\|_\infty$, as shown in Table 4. The error values are computed through the percentage difference with reference to the previous mesh. No error value is exhibited for Mesh A because this is the first mesh refinement used. So, the element sizes adopted here correspond to the Mesh C.

Table 4. Mesh refinement study.

Mesh	Cells	Infinity norm	Error (%)
Mesh A	193,597	10.0558	—
Mesh B	225,587	10.2309	4.79
Mesh C	343,935	10.5191	6.14
Mesh D	474,374	10.5688	1.03

In face of the interest in blade vicinity region, further refinement is imposed specifically at blades faces and a surrounding domain, where prismatic layers are positioned with the intention of detect flow behavior in the boundary layer region. The boundary layer thickness is predicted using Eq. 30 (Hansen, 2015). This prediction varies from 0.4252 mm to 0.5479 mm according to the analyzed flow rate. In Eq. 30, δ is the boundary layer thickness, x is the reference length, witch is considered as the mean chord of the blade, and Re is the Reynolds number.

$$\frac{\delta}{x} = \frac{0{,}382}{Re^{1/5}}, \tag{30}$$

The model validation is conducted by comparing the numerical results of the CFD simulations to the field measurements of the process variables. Pressure read on the turbine meter upstream, with a calibrated manometer, is confronted with the calculation results of the numerical solution. The pressures for the flow rates of 80 and 120 m³/h are obtained from field measurement, and they are the same. The error of the validation results are presented in Table 5, and the comparison between field data and simulated are depicted in Figure 13 for a better visualization.

Computational cost for each studied flow rate is presented in Table 6.

Table 5. Numerical results compared to the field measurement values.

Flow rate (m³/h)	p_{CFD} (kPa)	p_{field} (kPa)	Relative error (%)
80	1491.41	1569.06	4.95
120	1531.73	1569.06	2.38
160	1494.03	1529.84	2.34
200	1554.80	1593.58	2.43
240	1498.12	1544.55	3.01
280	1402.72	1471.00	4.64

Table 6. Computational cost.

Flow rate (m³/h)	CPU time (minutes)
80	251
120	252
160	243
200	277
240	518
280	156

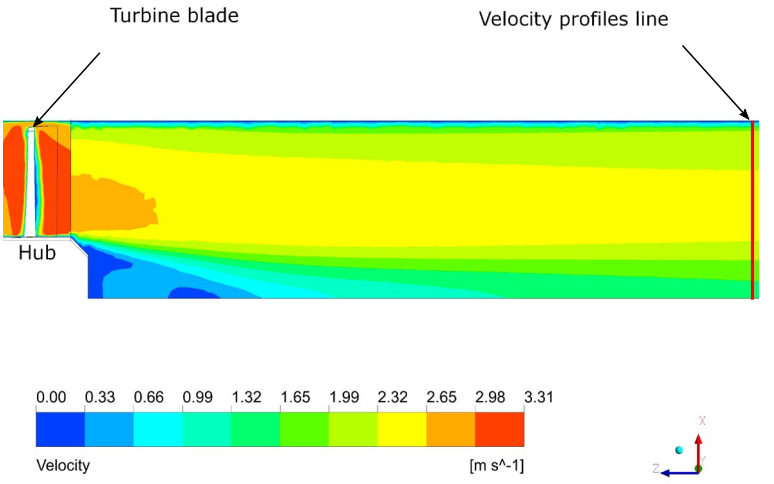

(a)

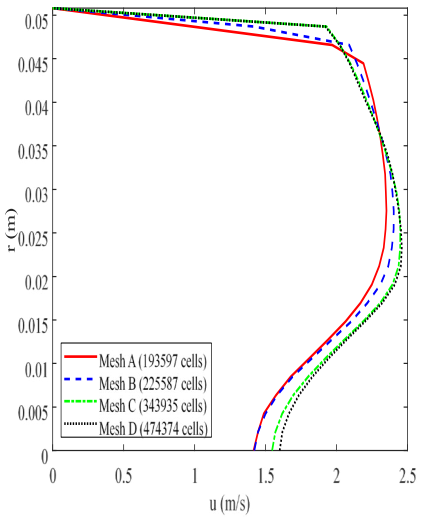

(b)

Figure 12. Velocity profile convergence with mesh refinement.

3.3. Velocity profiles

Velocity profiles are obtained from CFD simulations, specifically at the region of the fluid contact with the blades leading edge. The profiles are used as input data to the calculation of hydrodynamic torque for each flow rate simulated in the BET method. With the proposal of detecting velocity profiles at a section just before the entrance of the rotational domain, the profiles are extracted in a section located 4 mm upstream the turbine. In Figure 14, the velocity profiles obtained in an annular region for each one of the 6 operational conditions defined in Table 3 are presented. Vertical red line immediately before the rotational subdomain in Figure 14(a) indicates the position where the velocity profiles are extracted from the CFD results. The velocity distributions shown in Figure 14(b) correspond to 80 m³/h flow rate.

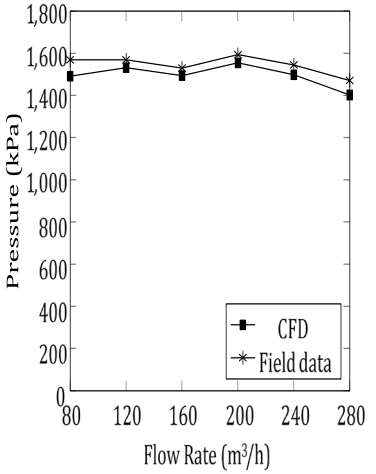

Figure 13. Model validation.

3.4. Cascade effect correction

In the proposed formulation, Eq. 25, the cascade effect is corrected by adding a constant k_c, through which the streamlines between two blades are corrected, consequently altering lift and drag coefficients. This correction aims to consider the distortion in streamlines that cross the blade sections. Different $k_c$values are found to be more suitable to better reproduce the field values of angular velocities for each one of the simulated flow rates. Considering the results for 120, 200 and 280 m³/h flow rates, Figures 15(a), (c) and (e) show the variation of lift coefficient with the local solidity, where C_l is the flat plate lift coefficient for unconstrained flow and C_{lc} is the lift coefficient corrected due to the cascade effect through the approach proposed in this paper. Figures 15 (b), (d) and (f) present the same results for the drag coefficients. Note that, in steady state regime, lift and drag coefficients do not change in relation to the local solidity. This is because the relative velocity on each blade section remains constant, keeping both angle of attack and Reynolds number also locally constants. The results confirm the conclusion of the work of Fagbenro (2013) that the local solidity has a big impact on the lift and drag generated on cascade of airfoils. As discussed in subsection 2.3, the increase of the local solidity indeed reduces lift and drag coefficients. This result is important because if the effect of streamline distortion is not considered in multiple bladed rotors, the performance of the turbine flowmeter can be overestimated.

3.5. Angular velocity and linearity results

Applying the solution method described in subsections 2.1 and 2.3, it is possible to obtain the value of angular velocity for which the numerical solution of Eq. 16 converges. The calculation procedure is repeated for each one of the six operational flow rates for which field data are available. With the proper adjustment of the constant *kc*, defined in Eq. 25, the model proposed allows the precise reproduction of the angular velocity values acquired in field measurements. Table 7 exhibits the comparison between the field measured angular velocities and the calculated results as well as the adjusted values of *kc* for each flow rate. The flow rates range shown in Table 7 is used because this is the range set in the studied industrial plant. It is observed that the value of *kc* presents small variation from the mean value of 0.9429, with standard deviation of 0.0036 within the operational range simulated. Figure 16 shows the variation of the differences between the adjusted values of *kc* and the mean value for different flow rates.

The accurate reproduction of the angular velocities obtained in the field measurement allows the simulation of the meter performance. API MPMS recommends the calculation of the linearity over the manufacturers' specified range, as

$$linearity = \frac{max\ kfactor - min\ kfactor}{mean\ kfactor} \times 100\% \quad (31)$$

Considering the k-factor values presented in Table 7, the linearity of the studied turbine can be calculated and the result is 0.11 %. This linearity meets the specification of the manufacturer manual, that establishes the limits of ±0.15 %. So, the calculation method proposed reveals adequacy for the simulation of meter performance.

Another relevant achievement is found when the results for the angular velocity obtained using the proposed method are compared to that from BET without considering the cascade effect. Figure 17 illustrates the comparison between measured values of angular velocity and the calculated results, corrected and uncorrected due to the cascade effect. Note that the proposed correction promotes major changes on the values obtained through BET. Taking the results for 80 m³/h flow rate, which represent the minimum difference, the angular velocity for the uncorrected model is 3.6 times higher than the result considering the cascade effect correction. This discrepancy demonstrates that, without considering lift and drag corrections into BET model, resultant from the flow restricted in multiple bladed rotors, the angular velocities are overestimated. The comparison between the present work and the measured values is shown in Figure 17, confirming the model ability to precisely predict the performance of the turbine flowmeter. This result is obtained using the adjusted values of *kc* described in Table 7.

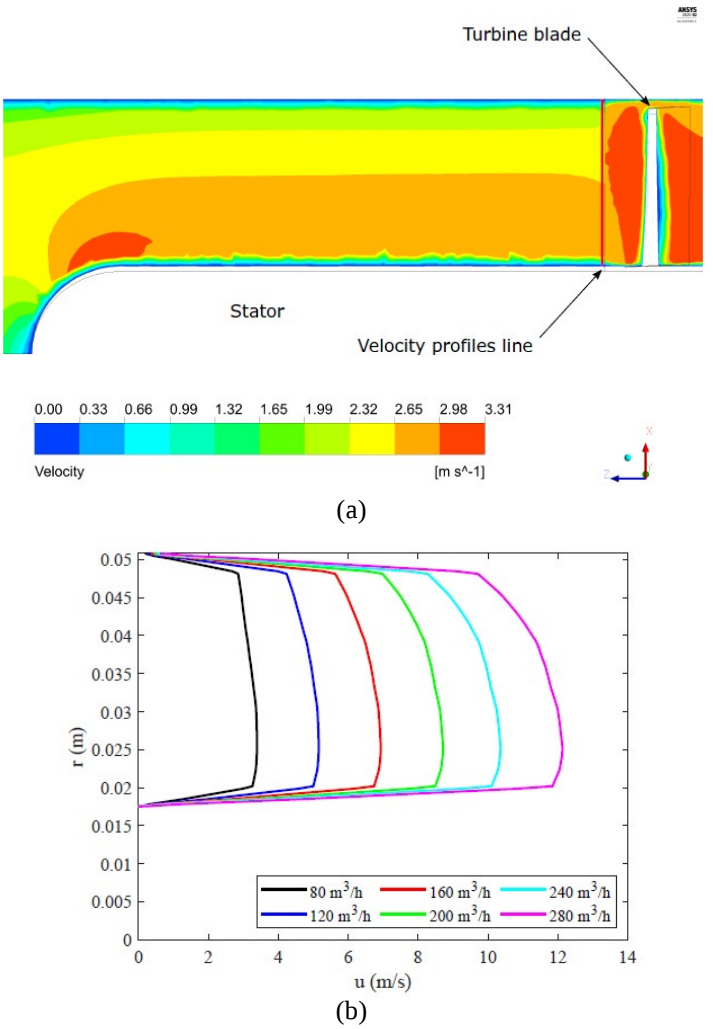

Figure 14. Velocity profiles for different operational flow rates.

Table 7. Values of parameter for different flow rates.

Flow rate (m^3/h)	Measured ω_T (rad/s)	Calculated ω_T (rad/s)	k_c
80	37.15	37.15	0.9364
120	55.77	55.77	0.9418
160	74.38	74.38	0.9446
200	92.98	92.98	0.9469
240	111.55	111.55	0.9434
280	130.15	130.15	0.9443

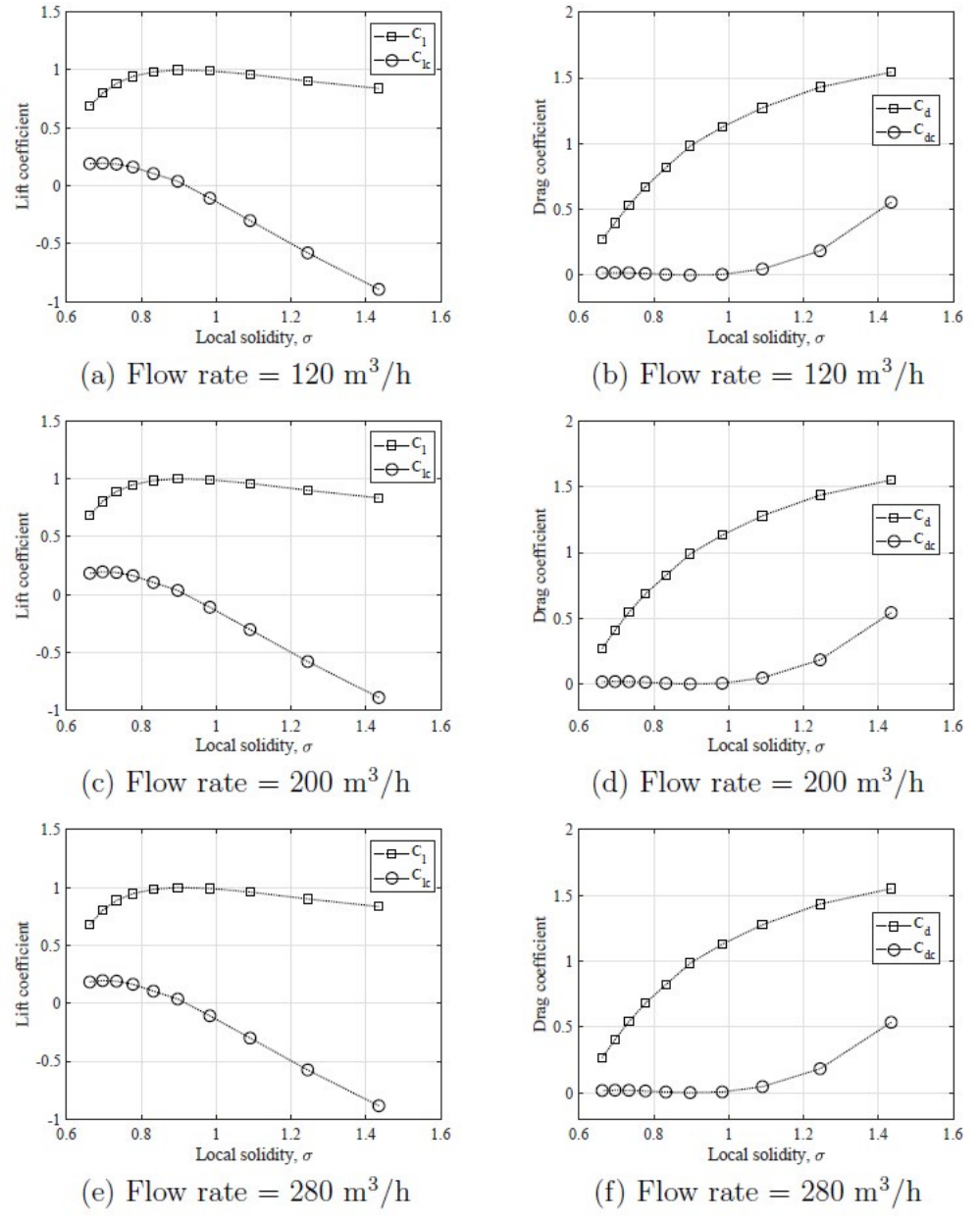

Figure 15. Lift and drag coefficients, varying with local solidity.

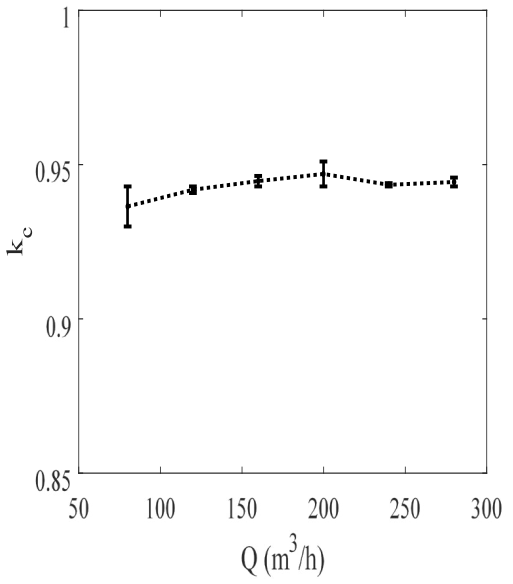

Figure 16. Variation of parameter k_c from mean value for different flow rates.

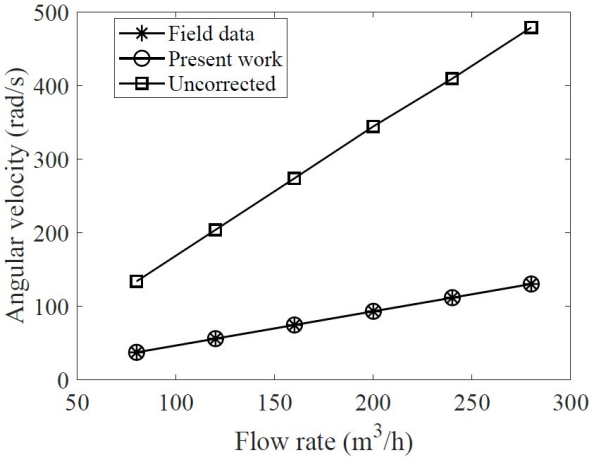

Figure 17. Angular velocity results.

4. Conclusions

In face of the wide acceptance and great applicability of turbine flowmeters in industry (Barajas Herrera et al., 2006), a new mathematical model to predict hydrodynamic behavior of such meters is proposed. One of the advantages of the model is the use of the BET, which generally agrees well with experimental data, as stated in Moreira et al. (2020). The BET model has also low computational cost and easy numerical implementation when compared to CFD techniques, as further explained in Vaz & Wood (2016). Additionally, the proposed model has the advantage of implementing a novel approach to consider the cascade effect correction. Such a correction is not considered in other works in the literature (Xu, 1992a; Xu, 1992b; Saboohi et al., 2015; Hariri et al., 2015; Dzemic et al., 2018). From the geometrical characteristics of the studied meter and physical properties of the fluid, typical operational conditions are simulated using CFD to provide input data necessary to the BET calculation. Considering the relatively high density of blades in the turbine flowmeter, the procedure proposed in this work included a correction to the cascade effect, based on experimental results of restrained flow in wind tunnels. The cascade effect correction is implemented by means of a correction for the angle of attack along the blade length. The correction formulation includes a parameter, k_c, dependent on the geometric aspects of the blade hydrofoil, which promotes distortions on the streamline crossing the blade section. Results obtained from the calculation methodology proposed here revealed that, with proper adjustment of parameter k_c, it is possible to reproduce the angular velocities obtained in field measurements with the studied turbine flowmeter. Consequently, the model is capable of predicting the performance of the equipment with satisfactory agreement. On the other hand, if the cascade effect is not considered in the BET analysis, the performance of the turbine can be overestimated. The main contribution of this work is to propose a mathematical tool to technically subsidy possible adjustments of operational parameters of measurement systems aiming enhancements in productivity and efficiency in LPG industries. It is worth noting that the present model is not applicable only for LPG, but for any axial turbine, specially with multiple blades, changing only the fluid properties. The model proposed revels to be innovative once it combines analytical techniques classically applied to wind and hydrokinect turbines with corrections due to the cascade effect to the development of a solution strategy applied to turbine flowmeters.

References

American Petroleum Institute. (2005). Chapter 5.3. Measurement of Liquid Hydrocarbons by Turbine Meters. En: *Manual of Petroleum Measurement Standards*. (5th ed.). API Publications.

Andriotis, A., Gavaises, M., Arcoumanis, C. (2008). Vortex flow and cavitation in diesel injector nozzles. *Journal of Fluid Mechanics, 610*, 195-215. https://doi.org/10.1017/S0022112008002668

Baker, R.C. (1991). Turbine and related flowmeters: I. Industrial practice. *Flow Measurement and Instrumentation*, *2*(3), 147-161. https://doi.org/10.1016/0955-5986(91)90027-O

Baker, R.C. (1993). Turbine flowmeters: II. theoretical and experimental published information. *Flow Measurement and Instrumentation, 4*(3), 123-144. https://doi.org/10.1016/0955-5986(93)90048-N

Barajas Herrera, E. J., Pérez, J. C., Barrero, J. G., Roncansio, R., & Luque Ortiz, I. (2006). Desarrollo e implementación de computadores de flujo. *Fuentes, El reventón energético*, *4*(1). https://revistas.uis.edu.co/index.php/revistafuentes/article/view/973

Brennen, C.E. (2016). *Internet Book on Fluid Mechanics*. Dankat Publishing. http://brennen.caltech.edu/fluidbook/

Caldas, A., Caldas, A., Dos Santos, C., Ochoa, A., Cezar, K., Michima, P. (2020). Design, development and construction of hall effect-based turbine meter type to measure flow in low-cost lithium bromide salt: Proposed flowmeter and first results. *International Journal of Refrigeration*, *112*, 240-250. https://doi.org/10.1016/j.ijrefrig.2020.01.002

Daniel Measurement and Control, Inc. 2005. *Daniel UMB Turbine meter. Installation and Operation manual.* Part Number 3-9008-501. Revision B. Houston, Texas.

Dzemic, Z., Sirok, B., & Bizjan, B. (2018). Turbine flowmeter response to transitional flow regimes. *Flow Measurement and Instrumentation, 59*, 18-22. https://doi.org/10.1016/j.flowmeasinst.2017.11.006

Fagbenro, K. A. (2013). *Cascade Effects on Circular Arc Airfoils for Windmill Analysis* [Master's thesis, University of Calgary, Calgary, Canada] https://doi.org/10.11575/PRISM/25220

Guo, S., Sun, L., Zhang, T., Yang,W., & Yang, Z. (2013). Analysis of viscosity effect on turbine flowmeter performance based on experiments and CFD simulations. *Flow Measurement and Instrumentation, 34*, 42-52. https://doi.org/10.1016/j.flowmeasinst.2013.07.016

Hansen, M. (2015). *Aerodynamics of wind turbines*. (3ra ed.). Routledge.

Hariri, S., Hashemabadi, S.H., Noroozi, S., Rostami, A. (2015). Analysis of operational parameters, distorted flow and damaged blade effects on accuracy of industrial crude oil turbine flow meter by CFD techniques. *Journal of Petroleum Science and Engineering*, *127*, 318-328. https://doi.org/10.1016/j.petrol.2015.01.010

Ji, B., Luo, X., Arndt, R.E., & Wu, Y. (2014). Numerical simulation of three dimensional cavitation shedding dynamics with special emphasis on cavitation-vortex interaction. *Ocean Engineering, 87*, 64-77. https://doi.org/10.1016/j.oceaneng.2014.05.005

Laws, N.D., & Epps, B.P. (2016). Hydrokinetic energy conversion: Technology, research, and outlook. *Renewable and Sustainable Energy Reviews, 57*, 1245-1259. https://doi.org/10.1016/j.rser.2015.12.189

Limacher, E., Morton, C., & Wood, D. (2016). On the trajectory of leading-edge vortices under the influence of coriolis acceleration. *Journal of Fluid Mechanics, 800*, R1. https://doi.org/10.1017/jfm.2016.395

Limacher, E., & Rival, D.E. (2015). On the distribution of leading-edge vortex circulation in samara-like flight. *Journal of Fluid Mechanics, 776,* 316-333. https://doi.org/10.1017/jfm.2015.279

Moreira, J.L., Mesquita, A.L., Araujo, L.F., Galhardo, M.A., Vaz, J.R., & Pinho, J.T. (2020). Experimental investigation of drivetrain resistance applied to small wind turbines. *Renewable Energy,* 153, 324-333. https://doi.org/10.1016/j.renene.2020.02.014

Salami, L.A. (1984). Effect of upstream velocity profile and integral flow straighteners on turbine flowmeters. *International Journal of Heat and Fluid Flow, 5*(3), 155-165. https://doi.org/10.1016/0142-727X(84)90073-0

Saboohi, Z., Sorkhkhah, S., & Shakeri, H. (2015). Developing a model for prediction of helical turbine flowmeter performance using CFD. *Flow Measurement and Instrumentation, 42*, 47-57. https://doi.org/10.1016/j.flowmeasinst.2014.12.009

Selig, M.S., Guglielmo, J.J., Broeren, A.P., & Giguere, P. (1995). *Summary of Low-Speed Airfoil Data*. (Vol. 1). SoarTech Publications.

Rio Vaz, D.A.T.D., Vaz, J.R.P., Silva, P.A.S.F. (2018). An approach for the optimization of diffuser-augmented hydrokinetic blades free of cavitation. *Energy for Sustainable Development, 45*, 142-149. https://doi.org/10.1016/j.esd.2018.06.002

Vaz, J. R., & Wood, D. H. (2016). Aerodynamic optimization of the blades of diffuser-augmented wind turbines. *Energy Conversion and Management,* 123, 35-45. https://doi.org/10.1016/j.enconman.2016.06.015

Vaz, J.R., Wood, D.H., Bhattacharjee, D., & Lins, E.F. (2018). Drivetrain resistance and starting performance of a small wind turbine. *Renewable energy, 117*, 509-519. https://doi.org/10.1016/j.renene.2017.10.071

Wang, Y., Li, H., Liu, X., Li, L., Huang, C., & Hu, J. (2020). A new method of measuring the oil-air-water three-phase flow rate. *Chemical Engineering Communications, 207*(1), 1-16. https://doi.org/10.1080/00986445.2016.1246438

Wood, D. (2011). Small wind turbines. In: *Advances in wind energy conversion technology*. (pp. 195-211). Springer. https://doi.org/10.1007/978-3-540-88258-9

Xu, Y. (1992a). Calculation of the flow around turbine flowmeter blades. *Flow Measurement and Instrumentation, 3*(1), 25-35. https://doi.org/10.1016/0955-5986(92)90013-U

Xu, Y. (1992b). A model for the prediction of turbine flowmeter performance. *Flow Measurement and Instrumentation,* 3(1): 37-43. https://doi.org/10.1016/0955-5986(92)90014-V

List of acronyms and abbreviations

API	American Petroleum Institute
BET	Blade Element Theory
CFD	Computational Fluid Dynamics
LPG	Liquefied Petroleum Gas
MPMS	Manual of Petroleum Measurement Standards

Nomenclature

a	axial induction factor
a'	tangental induction factor
B	number of blades
c	chord
C_d	drag coefficient
C_{dc}	corrected drag coefficient
C_f	friction coefficient
C_l	lift coefficient
C_{lc}	corrected lift coefficient
$C_{m,c/4}$	momentum coefficient at 1/4 of chord
C_n	normal force coefficient
C_t	tangential force coefficient
D_r	drag force
e	clearance between rotor and sleeve
F_n	normal force
F_t	tangential force
h_{ts}	test section height
J_T	mass momentum of inertia
k	k-factor
k_c	cascade effect correction factor
l	sleeve thickness
L_i	lift force
r	radius
r_b	sleeve inner radius
r_h	hub radius
R	rotor radius
T_D	dissipative torque
T_T	hydrodynamic torque
U	centerline velocity
V	velocity
W	relative velocity
α	angle of attack
α_c	corrected angle of attack
α_u	uncorrected angle of attack
δ	boundary layer thickness
θ	twist angle
σ	local solidity
σ_c	corrected angle of attack
ϕ	flow angle
ω	velocidade angular / dissipação específica
ω_T	velocidade angular da turbina